ELSEVIER

Journal of Alloys and Compounds 315 (2001) 259–264

Journal of ALLOYS AND COMPOUNDS

www.elsevier.com/locate/jallcom

Crystal structure, electronic structure, and magnetic properties of bismuth-strontium ferrites

J. Li*, Y. Duan, H. He, D. Song

Institute of Materials Science and Engineering, Lanzhou University, Lanzhou 730000, China

Received 14 August 2000; accepted 30 October 2000

Abstract

$Bi_{1-x}Sr_xFeO_3$ compounds were studied by X-ray diffraction, Mössbauer effect, and magnetic measurements. The replacement of trivalent Bi by divalent Sr leads to a change of the lattice symmetry from the rhombohedrally distorted perovskite of $BiFeO_3$ to the cubic one of $SrFeO_{2.97}$ and results in oxygen deficiency in the lattice. The oxygen-deficient $Bi_{1-x}Sr_xFeO_3$ compounds have two different crystal sites for iron ions, i.e., the octahedral sites and the oxygen-deficient tetrahedral sites. However, the iron ions both on the octahedral sites and the tetrahedral sites are in the trivalent state. $Bi_{1-x}Sr_xFeO_3$ exhibits the presence of both antiferromagnetic and weak ferromagnetic interactions simultaneously. As the Sr content increases, the susceptibility and magnetization of $Bi_{1-x}Sr_xFeO_3$ decrease.

Keywords: Oxide materials; Transition metal compounds; Magnetically ordered materials; Mössbauer spectroscopy; Magnetic measurements

1. Introduction

Since the discovery of high temperature superconductivity in the perovskite-related copper oxide and colossal magnetoresistance effect in the perovskite-type manganates [1], there has been renewed interest in intermediate valence or mixed valence perovskite compounds. In order to obtain new materials with special electronic structures and special properties as well as to understand physical mechanisms of the family of perovskite-related transition metal oxide functional materials, perovskite-type iron oxides $R_{1-x}M_xFeO_3$ were composed by partially substituting the trivalent rare earths R^{3+} in $RFeO_3$ by the divalent metals M^{2+} with ionic radii near those of the rare earths.

Depending mainly on the ionic radius difference between R^{3+} and M^{2+} and the synthesis processes, the substitution of R^{3+} in $RFeO_3$ by M^{2+} may have at least three possible consequences: (1) $R_{1-x}M_xFeO_3$ can consist of two or more phases, as in the case of $La_{1-x}Ba_xFeO_3$ [2,3]. (2) Iron in $R_{1-x}M_xFeO_3$ has an intermediate valence, which increases gradually from trivalent iron to tetravalent iron with increasing x, as in the case of $La_{1-x}Ca_xFeO_3$ [4,5]. (3) Iron in $R_{1-x}M_xFeO_3$ remains in the trivalent state, and as a result, oxygen deficiency occurs in the lattice to electrically neutralize the compounds, as in $Sm_{1-x}Ca_xFeO_3$ [6,7].

Bismuth ferrite, $BiFeO_3$, has been an attractive magnetoelectric material, since it is ferroelectric (Curie temperature T_c about 1123 K) [8] and has a cycloidal spiral magnetic ordering [9]. $BiFeO_3$ is reported to have a rhombohedrally distorted perovskite structure with $a=3.96$ Å and $\alpha=89°28'$ belonging to the space group $R3c$ [8,10,11]. $BiFeO_3$ yields a six-line Mössbauer spectrum at room temperature with a hyperfine field of 49.3 T [12]. Its Néel temperature T_N was determined to be about 640 K [12]. Strontium ferrite, $SrFeO_3$, prepared in oxygen at high pressure was well known for containing only tetravalent iron [13]. Its crystal structure was accurately determined recently. $SrFeO_x$ ($2.90 \leq x \leq 3.00$) has a cubic perovskite structure belonging to the space group $Pm3m$ and a lattice constant of 3.8553 Å when $x=2.97$ [14]. $SrFeO_3$ is an antiferromagnet having a screw spin structure and $T_N=134$ K [15,16]. However, no systematic study on the system $BiFeO_3$–$SrFeO_3$, i.e., the bismuth-strontium ferrites $Bi_{1-x}Sr_xFeO_3$, has been reported so far. As $BiFeO_3$ possesses the special magnetoelectric properties, it is of interest to study structures and properties of $Bi_{1-x}Sr_xFeO_3$.

Our present paper reports the synthesis of $Bi_{1-x}Sr_xFeO_3$ samples, the crystal structure and lattice constant determi-

*Corresponding author.

E-mail address: Lijg@lzu.edu.cn (J. Li).

0925-8388/01/$ – see front matter
PII: S0925-8388(00)01313-X

nation, and electronic structures of the compounds as well as the magnetic measurement results on the $Bi_{1-x}Sr_xFeO_3$ samples.

2. Experimental procedure

$Bi_{1-x}Sr_xFeO_3$ samples were prepared in air for $x=0.20$, 0.33, 0.40, 0.50, 0.60, and 0.67 by solid state reaction. Dry Bi_2O_3, $SrCO_3$, and Fe_2O_3 powders with purities of 99.5% or better were mixed in the atomic ratios of Bi:Sr:Fe=(1–x):x:1 by grinding and then pre-heated in air to 900°C for 30 h. The X-ray diffraction patterns of the pre-heated samples revealed that the starting substances had reacted. The pre-heated mixtures were ground again and pressed into pellets. The pellets of $x=0.20$, 0.33, and 0.40 were heated in air at 930°C for 72 h, followed by a slow cooling at a rate of 60°C/h down to 720°C. The pellets of $x=0.50$, 0.60, and 0.67 were heated in air at 1000°C for 72 h and cooled at a rate of 60°C/h down to 720°C. The samples were then tempered in air at 720°C for 100 h and cooled slowly at a rate of 60°C/h down to room temperature. The samples were heated at different temperatures to avoid melting but to ensure a complete reaction. The slow cooling and tempering at 720°C were thought to decrease oxygen deficiency in the samples and to let the samples approach their equilibrium state at room temperature. The samples were finally pulverized for the X-ray powder diffraction, Mössbauer effect, and magnetic measurements.

X-ray powder diffraction measurements were undertaken at room temperature (298 K) on a Rigaku D/max-2400 diffractometer with the standard goniometer of a radius of 185 mm. The Cu Kα radiation (40 kV, 40 mA), a divergence slit of 0.5°, a scatter slit of 0.5°, a receiving slit of 0.15 mm (0.046°), 2θ scan steps of 0.02°, and a curved-crystal graphite monochromator for the diffracted beam were used. The goniometer has been verified currently to have a 2θ precision of ±0.01° and a reproducibility of ±0.001° at 298 K. The measured data were recorded and analyzed with the help of a HP Apollo 9000 work station. The $K\alpha_2$ diffraction peaks were eliminated by the Rachinger's method [17]. The integral intensities of the $K\alpha_1$ diffraction peaks were obtained by least-square fitting of the $K\alpha_1$ peaks with Gaussian profiles. The backgrounds were removed in the intensity determination. The positions of the $K\alpha_1$ diffraction peaks were determined by a center-of-gravity method. The wave length of 1.54056 Å was employed in all calculations. In order to eliminate the systematic errors the silicon powder of a purity of 99.9999% was used as an external standard reference material. The lattice constant $a=5.43094$ Å of silicon (standard reference material 640b) recommended by the International Center for Diffraction Data was used in the calibrations. The diffraction peak positions of silicon calculated from its lattice constant were employed to calibrate the measured diffraction peak positions of silicon and further to calibrate the diffraction peak positions of the $Bi_{1-x}Sr_xFeO_3$ samples.

Mössbauer effect measurements were performed at room temperature in the standard transmission geometry using a source of ^{57}Co in a Rh matrix. The spectra were collected by a Wissel CMCA-2000 multichannel analyzer and fitted using a least-square refinement program. The velocity of the Mössbauer spectrometer was calibrated using a pure α-Fe absorber.

AC susceptibility and magnetization measurements were carried out using an AC+DC magnetometer of the Quantum Design Physical Property Measurement System (Model 6000). The measurements were made on the powder samples with $x=0.2$, 0.4, and 0.6. The zero field AC susceptibility was measured over the temperature range from 4.2 to 295 K at 300 Hz in a driving field of 1 Oe.

3. Results and discussion

3.1. Crystal structure

The measured X-ray powder diffraction data on $Bi_{1-x}Sr_xFeO_3$ with x between 0.20 and 0.67 are listed in Table 1. The samples yield the diffractograms having the

Table 1
Powder diffraction data for $Bi_{1-x}Sr_xFeO_3$

hkl	$x=0.2$			$x=0.33$			$x=0.4$			$x=0.5$			$x=0.6$			$x=0.67$		
	d_{obs} (Å)	d_{calc} (Å)	I (%)	d_{obs} (Å)	d_{calc} (Å)	I (%)	d_{obs} (Å)	d_{calc} (Å)	I (%)	d_{obs} (Å)	d_{calc} (Å)	I (%)	d_{obs} (Å)	d_{calc} (Å)	I (%)	d_{obs} (Å)	d_{calc} (Å)	I (%)
100	3.9533	3.9524	27	3.9464	3.9465	20	3.9429	3.9401	20	3.9673	3.9466	16	3.9395	3.9357	14	3.9326	3.9317	11
110	2.7940	2.7948	100	2.7906	2.7906	100	2.7890	2.7861	100	2.7991	2.7907	100	2.7839	2.7830	100	2.7822	2.7801	100
111	2.2805	2.2819	17	2.2794	2.2785	18	2.2772	2.2748	18	2.2827	2.2786	15	2.2728	2.2723	17	2.2717	2.2700	15
200	1.9755	1.9762	23	1.9682	1.9733	15	1.9682	1.9700	15	1.9755	1.9733	23	1.9682	1.9679	24	1.9658	1.9659	30
210	1.7681	1.7676	6	1.7624	1.7649	4	1.7617	1.7621	6	1.7649	1.7650	5	1.7598	1.7601	5	1.7579	1.7583	5
211	1.6135	1.6136	26	1.6099	1.6112	20	1.6099	1.6085	26	1.6119	1.6112	31	1.6068	1.6068	30	1.6057	1.6051	30
220	1.3973	1.3974	9	1.3969	1.3953	6	1.3955	1.3930	9	1.3955	1.3953	10	1.3914	1.3915	11	1.3903	1.3901	10
310	1.2500	1.2499	6	1.2447	1.2480	3	1.2450	1.2460	7	1.2470	1.2480	8	1.2436	1.2446	7	1.2431	1.2433	8
222	1.1402	1.1410	2	1.1395	1.1393	2	1.1393	1.1374	2	1.1385	1.1393	3	1.1363	1.1362	3	1.1355	1.1350	3
321	1.0566	1.0563	5	1.0557	1.0548	2	1.0521	1.0530	4	1.0538	1.0548	5	1.0516	1.0519	6	1.0509	1.0508	7

Table 2
Crystallographic parameter of $Bi_{1-x}Sr_xFeO_3$

x	0.2	0.33	0.4	0.5	0.6	0.67
a (Å)	3.9524	3.9465	3.9401	3.9466	3.9357	3.9317

same patterns as that of $SrFeO_{2.97}$ [14]. All of the observed diffraction peaks from the $Bi_{1-x}Sr_xFeO_3$ samples with x ranging from 0.20 to 0.67 were reasonably indexed on the basis of a cubic perovskite unit cell of $SrFeO_{2.97}$. No additional peaks were found, indicating that the samples synthesized are the single-phased cubic perovskite $Bi_{1-x}Sr_xFeO_3$ compounds with the same symmetry as $SrFeO_{2.97}$. $BiFeO_3$ has a rhombohedrally distorted perovskite structure. Our results show, however, that the partial substitution of Bi in $BiFeO_3$ by Sr changes the symmetry from rhombohedral to cubic and that the symmetry is unchanged while further substitution of Bi by Sr in $Bi_{1-x}Sr_xFeO_3$ from $x=0.20$ to 0.67.

In general, the increasing substitution of Bi by Sr in $Bi_{1-x}Sr_xFeO_3$ shifts all the diffraction peaks to higher angle, which is indicative of the decrease in the unit cell dimension. The lattice constants of the cubic perovskite $Bi_{1-x}Sr_xFeO_3$ compounds with x between 0.20 and 0.67 were calculated from the observed diffraction peaks by a program based on the Cohen's analytical least-squares method [18,19]. The lattice constant a of $Bi_{1-x}Sr_xFeO_3$ in variation with x is given in Table 2 and pictured in Fig. 1.

In the diffractometric measurements, the main systematic errors include source spot profile, flat-specimen error, specimen transparency, axial divergence, and receiving slit, and other errors include zero point setting, specimen-surface displacement, precision and reproducibility of the goniometer, and temperature alteration [20]. The calibration through the external standard reference material should mainly eliminate the systematic errors. The diffractometer could align its zero point automatically through an optical adjustment mechanism. To ensure specimen flatness and minimize specimen-surface displacement, the grooved glass sample holders were filled with the sample powders. The temperature alteration during the measurements was about ±1 K.

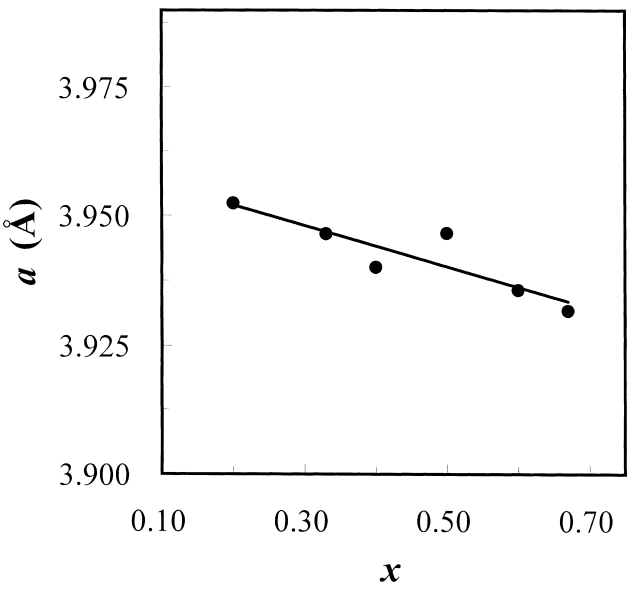

Fig. 1. The lattice constant a of $Bi_{1-x}Sr_xFeO_3$ as a function of the Sr content x.

The calculated interplanar distances d_{calc} are listed together with the measured data in Table 1. As shown in Fig. 1, in general, the lattice constant a of $Bi_{1-x}Sr_xFeO_3$ decreases almost linearly as x increases from 0.2 to 0.67, indicating that the substitution of Bi by Sr results in the decrease of the unit cell dimension.

The linear decrease of the lattice constant with increasing x in general can be understood by considering the effective ionic radius difference between Sr^{2+} and Bi^{3+}, the decreasing ionic radius of iron with increasing valence, and the oxygen deficiency.

The effective ionic radius of Sr^{2+} under the anion coordination number of 6 is 1.18 Å which is almost same as the effective ionic radius of 1.17 Å for Bi^{3+} [21]. This means that the ionic radius difference between Sr^{2+} and Bi^{3+} is very small and would hardly influence the lattice dimension. However, the increasing oxygen deficiency with increasing x would lead to the reduction of the unit cell dimension.

The deviation of the lattice constants for the $x=0.4$ and 0.5 samples from the general linear trend (Fig. 1) may arise from the synthesis condition. In our experiments, it was found that the melting point of $Bi_{1-x}Sr_xFeO_3$ increases with the increasing x. For simplicity and in order to avoid melting and reaction with the corundum crucibles, the samples with $x=0.2$, 0.33, and 0.4 were heated at 930°C; the samples with $x=0.5$, 0.6, and 0.67 were heated at 1000°C. However, 930°C may be relatively low for $x=0.4$, whereas 1000°C may be relatively high for $x=0.5$.

3.2. Electronic structure

Mössbauer spectra of $Bi_{1-x}Sr_xFeO_3$ for various x are reproduced in Fig. 2. Their Mössbauer parameter values are tabulated in Table 3. The $Bi_{1-x}Sr_xFeO_3$ compounds with different x show magnetic hyperfine splitting spectra. The magnetic hyperfine splitting spectra are indicative of magnetic ordering, most probably a screwed or slightly canted antiferromagnetic ordering as in $SrFeO_3$ or orthoferrites $RFeO_3$ [16,22]. The magnetic hyperfine splitting spectra measured at room temperature indicate that the Néel temperatures of $Bi_{1-x}Sr_xFeO_3$ are above room temperature. The $Bi_{1-x}Sr_xFeO_3$ compound of the $x=0.2$ composition yields a six-line spectrum with an isomer shift (IS) of 0.38 mm/s and a hyperfine field (H) of 50.0 T (Table 3). The isomer shift and hyperfine field of our $x=0.2$ sample are almost same as those of $BiFeO_3$ [12,23].

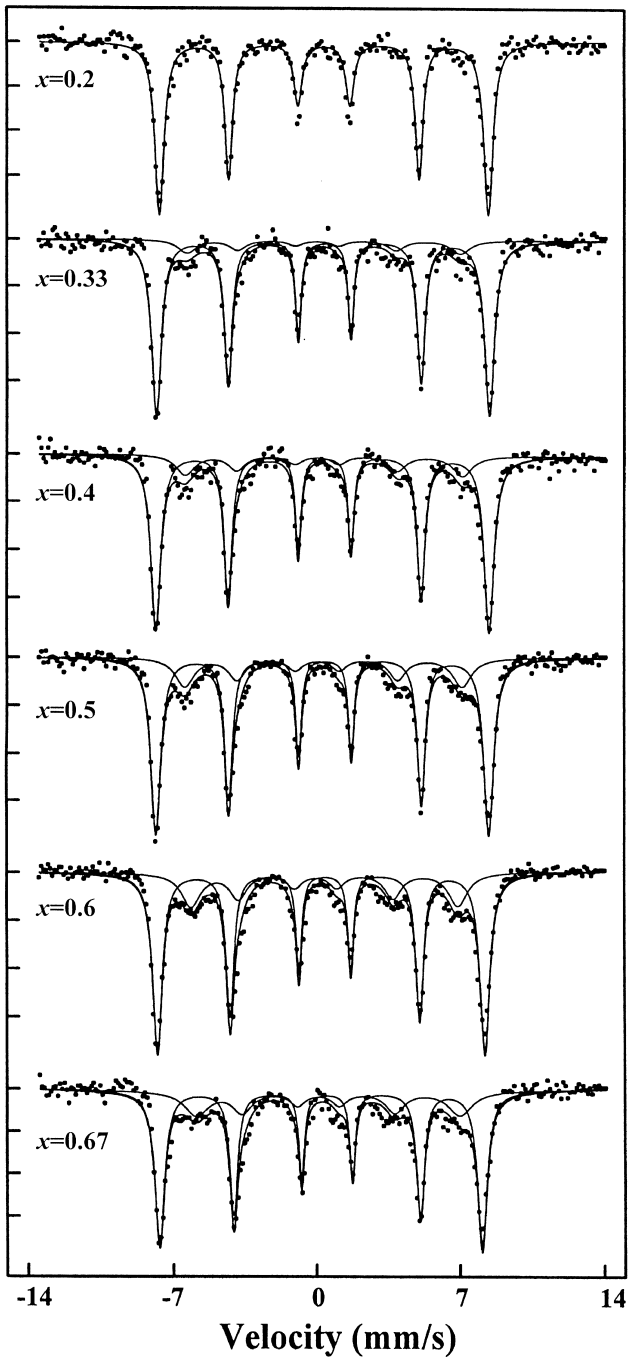

Fig. 2. The Mössbauer spectra of $Bi_{1-x}Sr_xFeO_3$ with various x measured at room temperature.

This implies that the iron in $Bi_{0.8}Sr_{0.2}FeO_3$ has almost the same valence state as in $BiFeO_3$. However, the zero quadrupole splitting of $Bi_{0.8}Sr_{0.2}FeO_3$ supports the high symmetry of a cubic crystal structure as determined by our X-ray diffraction studies, whereas the rhombohedral $BiFeO_3$ yields a quadrupole splitting as high as 0.37 mm/s [12]. Theoretically, the $x=0.2$ substitution of Sr for Bi should force the trivalent iron into an intermediate valence state between trivalence and tetravalence or to tetravalent ones. Unfortunately, this was not observed in our Mössbauer studies.

The Mössbauer spectra of the samples other than that of $x=0.2$ could be fitted with two six-line subspectra. Since only one phase exists in the $Bi_{1-x}Sr_xFeO_3$ samples, these two subspectra would come either from iron ions on two different lattice sites or from iron ions with different valence states. The substitution of divalent Sr for trivalent Bi in the single-phased $Bi_{1-x}Sr_xFeO_3$ may result in a change in valence state of iron or oxygen deficiency in lattice. The Mössbauer parameters of the one six-line subspectrum, i.e., the isomer shift around 0.22 mm/s, the quadrupole splitting around 0.34 mm/s, and the hyperfine field around 41 T, are those usually found for asymmetrically tetrahedrally surrounded trivalent iron in oxides [24]. The tetrahedral sites result from the oxygen deficiency. This indicates that the substitution of divalent Sr for trivalent Bi in $Bi_{1-x}Sr_xFeO_3$ leads to oxygen deficiency. The percentage of the subspectrum for iron on the tetrahedral sites increase with increasing x. This means that the increasing substitution leads to an increase of oxygen deficiency.

The other six-line subspectrum with the hyperfine field of about 50 T can be attributed to the iron ions on the octahedral sites. As x increases from 0.3 to 0.67, the isomer shift of this subspectrum decreases slightly from 0.38 to 0.35 mm/s. However, these isomer shift values still lie in the range for trivalent iron. The magnitude of the negative quadrupole splitting increases with increasing Sr content. The increasing substitution of Sr for Bi leads to an increase of oxygen deficiency. The increasing oxygen deficiency results in an increasing number of the tetrahedral sites of iron. The increasing number of the tetrahedral sites in the vicinity of the octahedral sites would make the octahedral sites electrically asymmetrical. Hence the magnitude of the negative quadrupole splitting increases with increasing Sr content.

3.3. Magnetic properties

Fig. 3 shows the temperature dependence of the AC susceptibility χ for $Bi_{1-x}Sr_xFeO_3$ of $x=0.2$, 0.4, and 0.6 from 295 to 4.2 K. The AC susceptibility increases slightly first with decreasing temperature, attains a maximum at T_m (temperature where χ is maximum), and then decreases. The slight rise in χ with decreasing temperature is a signature of weak ferromagnetic interactions setting in. The decrease of χ with decreasing temperature in the low temperature range indicates antiferromagnetic behavior. As the Sr content x increases from 0.2 to 0.6, the magnitude of χ decreases. The temperature for the maximum of χ, T_m, decreases from 140 to about 65 K as x increases from 0.2 to 0.4. T_m remains almost unchanged as x increases from 0.4 to 0.6.

Fig. 4 shows the magnetization curves for $Bi_{1-x}Sr_xFeO_3$ with $x=0.2$, 0.4 and 0.6 measured at 4.2 K. The mag-

Table 3
Mössbauer parameters of $Bi_{1-x}Sr_xFeO_3$

x	Fe (octahedral)				Fe (tetrahedral)			
	IS (mm/s)	QS (mm/s)	H (T)	%	IS (mm/s)	QS (mm/s)	H (T)	%
0.2	0.39	0	50.0	100				
0.33	0.38	−0.09	50.6	87	0.22	0.34	41.6	13
0.4	0.37	−0.11	50.7	81	0.22	0.34	42.2	19
0.5	0.37	−0.12	50.7	76	0.21	0.34	42.4	24
0.6	0.36	−0.22	49.8	73	0.22	0.35	40.9	27
0.67	0.35	−0.30	49.1	71	0.22	0.34	40.8	29

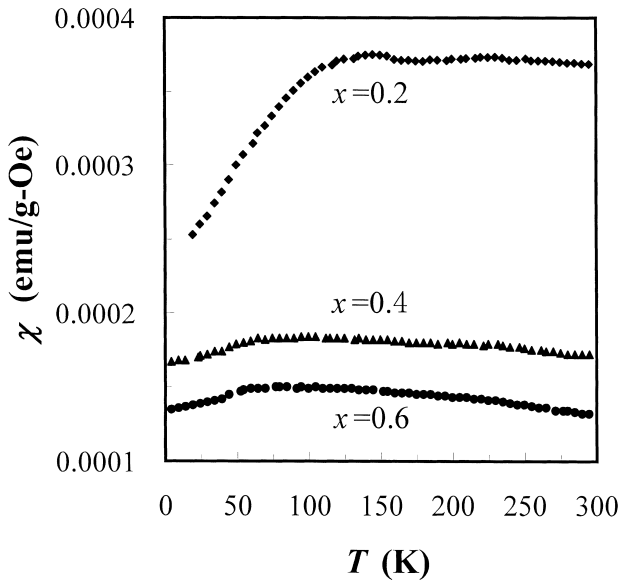

Fig. 3. The temperature dependence of AC susceptibility for $Bi_{1-x}Sr_xFeO_3$ with x=0.2, 0.4, and 0.6.

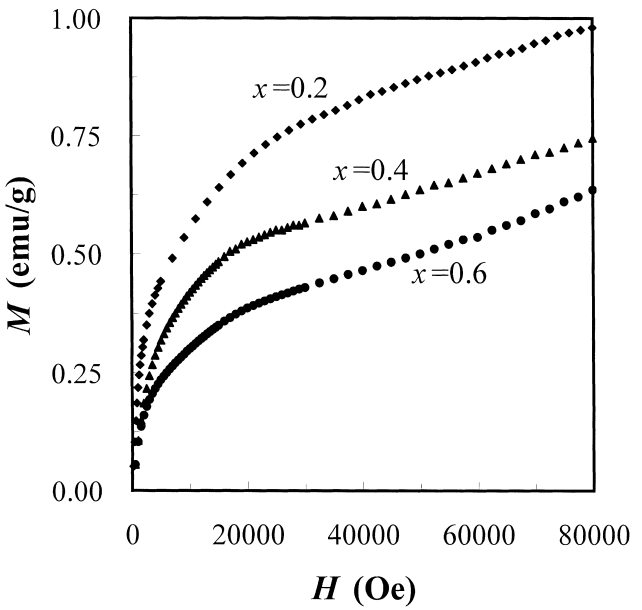

Fig. 4. The magnetization curves of $Bi_{1-x}Sr_xFeO_3$ with x=0.2, 0.4, and 0.6 measured at 4.2 K.

netization curves reveal a marked nonlinearity which is not expected from a pure antiferromagnet. However, such a behavior has been observed in many orthoferrites such as $LaFeO_3$. The curvature in the magnetization curves is understandable in terms of the presence of weak ferromagnetic interactions. A weak ferromagnetic order could arise from the non-collinear (canted) arrangement of spins in two sublattices [25]. In canted spin systems the antiferromagnetic ordering is observed along one axis and the ferromagnetic order along another axis. The magnetization curves show that the magnetization is unsaturated even at 80 000 Oe field. The increase in the divalent Sr content results in reduction of the magnetization.

According to the X-ray diffraction and Mössbauer effect study results, the increasing substitution of divalent Sr for Bi in $Bi_{1-x}Sr_xFeO_3$ leads to a decrease in the lattice dimensions and the increasing oxygen deficiency. All these will in turn influence magnetic interactions between Fe ions. As x increases, the number of the oxygen vacancies increases. Some octahedral coordinations of iron become the tetrahedral co-ordinations. When the coordination number of iron decreases from 6 to 4, the number of magnetic couplings decreases. Therefore, as x increases, the susceptibility and magnetization of $Bi_{1-x}Sr_xFeO_3$ decrease.

4. Conclusions

The $Bi_{1-x}Sr_xFeO_3$ samples for x ranging from 0.20 to 0.67 are the single-phased cubic perovskite compounds having the same symmetry as $SrFeO_{2.97}$. In general, the lattice constant of $Bi_{1-x}Sr_xFeO_3$ decreases almost linearly with x increasing from 0.20 to 0.67. This can be explained in terms of the increasing oxygen deficiency.

The iron ions in $Bi_{1-x}Sr_xFeO_3$ are located on the octahedral sites and tetrahedral sites. The substitution of Sr^{2+} for Bi^{3+} mainly results in oxygen deficiency in the lattice. The oxygen deficiency increases with the Sr content. The iron ions on the octahedral sites and on the tetrahedral sites are all in the trivalent state.

$Bi_{1-x}Sr_xFeO_3$ behaves like an antiferromagnet and a weak ferromagnet simultaneously. The presence of the antiferromagnetic and ferromagnetic order in

$Bi_{1-x}Sr_xFeO_3$ may be due to the presence of non-linear spin arrangement. As the Sr content increases, the susceptibility and magnetization of $Bi_{1-x}Sr_xFeO_3$ decrease. This can be explained by considering the increasing oxygen deficiency, which decreases the magnetic coupling number of some iron ions.

Acknowledgements

It is a pleasure to acknowledge Dr. G. Williams and Dr. A. H. Morrish for helpful discussions and help in performing the magnetic and Mössbauer effect measurements. This research received financial supports from the National Natural Science Foundation of China (NSFC), the Excellent Young Teacher Foundation, and the Key Teacher Foundation, both of Chinese Education Ministry. One of the authors (J.L.) wishes to thank the Canadian International Development Agency (CIDA) for funding the exchange visit at the University of Manitoba, Canada.

References

[1] S. Jin, T.H. Tiefel, M. McCormack, R.A. Fastnacht, R. Ramesh, L.H. Chen, Science 264 (1994) 413.
[2] J. Li, J. Jing, J. Mater. Sci. 27 (1992) 4361.
[3] J. Li, X. Cai, T.M. Wang, Appl. Phys. A 55 (1992) 158.
[4] J. Li, Phys. Scripta 45 (1992) 62.
[5] J. Li, in: E.M. McCarronIII, H.-C. Zur Loye, S.M. Kauzlarich, A.W. Sleight (Eds.), Solid State Chemistry of Inorganic Materials II, Vol. 547, Mat. Res. Soc. Symp. Proc. Mat. Res. Soc, Warrendale, 1999, p. 51.
[6] J. Li, X. Cai, X. Yang, T.M. Wang, Phys. Status Solidi B 179 (1993) 9.
[7] J. Li, J. Alloys Comp. 203 (1994) L1.
[8] C. Michel, J.M. Moreau, G.D. Achenbach, R. Gerson, W.J. James, Solid State Commun. 7 (1969) 701.
[9] I. Sosnowska, T. Peterlin-Neumaier, E. Steichele, J. Phys. C: Solid State Phys. 15 (1982) 4835.
[10] Yu.Ya. Tomashpolskii, Yu.N. Venevtsev, G.S. Zhdanov, Sov. Phys.-Crystallogr. 12 (1967) 209.
[11] J.M. Moreau, C. Michel, R. Gerson, W.J. James, J. Phys. Chem. Solids 32 (1971) 1315.
[12] A. Biran, P.A. Montano, U. Shimony, J. Phys. Chem. Solids 32 (1971) 327.
[13] P.K. Gallagher, J.B. MacChesney, D.N.E. Buchanan, J. Phys. Chem. 41 (1964) 2429.
[14] Y. Takeda, K. Kanno, T. Takada, O. Yamamoto, M. Takano, N. Nakayama, Y. Bando, J. Solid State Chem. 63 (1986) 237.
[15] J.B. MacChesney, R.C. Sherwood, J.E. Potter, J. Phys. Chem. 43 (1965) 1907.
[16] T. Takeda, Y. Yamaguchi, H. Watanabe, J. Phys. Soc. Japan 33 (1972) 967.
[17] W.A. Rachinger, J. Sci. Instrum. 25 (1948) 254.
[18] M.U. Cohen, Rev. Sci. Instrum. 6 (1935) 68.
[19] M.U. Cohen, Rev. Sci. Instrum. 7 (1936) 155.
[20] P. Klug, L.E. Alexander, X-Ray Diffraction Procedures for Polycrystalline and Amorphous Materials, John Wiley & Sons, New York, 1974, p. 290 and 606.
[21] R.D. Shannon, Acta Cryst. A 32 (1976) 751.
[22] D. Treves, J. Appl. Phys. 36 (1965) 1033.
[23] C. Blaauw, F. van der Woude, J. Phys. C: Solid State Phys. 6 (1973) 1422.
[24] H.J. Whitefield, Aust. J. Chem. 20 (1967) 859.
[25] J.L. Dormann, M. Nogues, J. Phys.: Condens. Matter. 2 (1990) 1223.